AIMS Mathematics, 10(7): 15867–15892.
DOI: 10.3934/math.2025711
Received: 28 April 2025
Revised: 22 June 2025
Accepted: 01 July 2025
Published: 14 July 2025

https://www.aimspress.com/journal/Math

Research article

Finite element method for Poisson equations with the Wang-Ball element

Lanyin Sun* **and Ziwei Dong**

School of Mathematics and Statistics, Xinyang Normal University, Xinyang, 464000, China

* **Correspondence:** Email: lysun@xynu.edu.cn.

Abstract: In electrostatic field research, the Poisson equation is the core equation describing the relationship between electric potential and charge distribution. The finite element method (FEM) is an analytical engineering tool for accurately calculating various physical quantities in the electrostatic field. In this paper, we employ the Wang-Ball basis functions to construct the trial and test function spaces of FEM for solving the Poisson equation. In addition, we provide an error analysis based on the Wang-Ball operator. Several examples with different electrostatics backgrounds are also given to substantiate the effectiveness of this method. Furthermore, numerical results show that Wang-Ball elements work well for degree $k > 3$.

Keywords: finite element method; the Wang-Ball element; Poisson equation; unisolvence; error analysis
Mathematics Subject Classification: 65D17, 65M60

1. Introduction

Electrostatics [1] describes the distribution of the electric field generated by stationary charges through Coulomb's law and Gauss's theorem. The Poisson equation [2] ($-\nabla^2\Phi = \frac{\rho}{\varepsilon_0}$) is its core mathematical expression. It directly relates the charge density ρ to the spatial variation of the electric potential Φ, transforming the complex problem of vector fields into the solution of a differential equation of a scalar field. The Laplacian operator $\nabla^2\Phi$ describes the comprehensive situation of the spatial variation rate of the electric potential Φ. From a physical perspective, it reflects the degree of curvature or the nonuniformity of the change in the electric potential in all directions in space [3]. The charge density ρ represents the distribution of charges in space, and the Poisson equation indicates that the Laplacian value of the electric potential at a certain point in space is directly related to the charge density at that point. That is to say, the presence of charges will cause a change in the spatial distribution of the electric potential. Here, ε_0 is a constant related to the properties of a vacuum, which measures the degree of response of the vacuum to an electric field.

The study of the Poisson equation in electrostatics has a long history. In 1973, Srebrenik [4] presented an analytic expression for the total potential in atomic and molecular systems, where the potential function was derived from the analytic solution of the Poisson equation. A new three-dimensional (3D) numerical solution of the full Poisson equation was explored by Schnitzer and Lambrakis [5] using the finite difference method (FDM) in 1991, aiming to simulate the electrostatic interaction between charged molecules and non-uniform dielectric bodies. In 2009, Hu et al. [6] relied on the analytical solution of the Poisson equation to conduct an in-depth investigation of the electrostatic integrity of ultrathin-body germanium-on-insulator metal oxide semiconductor field-effect transistors. In 2012, Storey and Bazant [2] considered the situation where the mean-field approximation failed and developed a fourth-order modified Poisson equation, which was helpful for explaining the suppression of the induced charge electrokinetic phenomenon at high salt concentrations. In 2024, Salem and Aldabbagh [7] solved the Poisson equation through FDM to estimate the electrostatic field and electric potential of an axially symmetric Gaussian charge distribution.

Solving the Poisson equation in the electrostatic field can not only thoroughly reveal the theoretical laws of the generation and distribution of the electric field, but also plays a core role in practical applications such as improvement of the performance of electronic devices and the guarantee of electrostatic safety, thus possessing great research value. There are many methods for solving the Poisson equation, including the FDM [8], the finite element method (FEM), and the method of particular solutions [9]. The FEM is an engineering tool that can effectively calculate problems such as the distribution of the electrostatic field and capacitance in charged objects with complex shapes and different media. In 1982, Arnold [10] formulated and analyzed a novel semidiscrete FEM with discontinuous elements dedicated to the numerical solution of nonlinear parabolic boundary value problems. In 1990, Guedes and Kikuchi [11] explored homogenization techniques to calculate the effective elastic moduli of composite materials using finite element analysis and an adaptive FEM. In 2000, Strouboulis et al. [12] presented the generalized FEM by integrating the FEM and the partition of unity method. Logg [13] reviewed studies on the fully automated FEM and discussed algorithms for efficient, automatic computation of discrete equations from a specific variational problem in 2007. The FEM was utilized by Baghbani et al. [14] to construct two-dimensional (2D) models for both existing and new tunnels with varying diameters in 2024.

The FEM can accurately solve the Poisson equation in the electrostatic field, which is of indispensable significance for accurately analyzing physical quantities such as the electric field distribution and electric potential. The automatic 3D mesh generation system for molecular geometries, which was developed by Cortis and Friesner [15] in 1997, was employed to solve the Poisson-Boltzmann (PB) equation via the FEM. In 2006, Hsu et al. [16] explored a parallel electrostatic Poisson equation solver coupled with parallel adaptive mesh refinement using the Galerkin FEM with a tetrahedral mesh. In 2012, Holst et al. [17] focused on the development of an efficient and dependable adaptive FEM tailored specifically for the nonlinear PB equation. A linearized local conservative mixed FEM was proposed and analyzed by Gao and Sun [18] in 2018 for the Poisson-Nernst-Planck equations, with a new vector-valued variable, the potential flux, being introduced specifically for the Poisson equation. In 2024, Guo et al. [19] proposed a numerical simulation code called the 2D finite element electron gun to simulate and analyze fine pencil beams by utilizing the FEM to solve the Poisson equation and generate an axisymmetric electrostatic field solver.

When using the FEM to solve the Poisson equation, the basis functions play a very important role, which can directly affect the stability and accuracy of the solutions. B-spline basis functions, a cornerstone in computational geometry, were pioneered by de Boor [20] and Cox [21] in 1972, laying the theoretical foundation for geometric modeling. Subsequently, Kagan et al. [22] validated their feasibility in a FEM for geometric design and mechanical analysis. Building upon this, in 2005, Hughes et al. [23] revolutionized the field by introducing isogeometric analysis through nonuniform rational B-splines (NURBS) basis functions, bridging computer-aided design and numerical simulation.

The Ball basis functions possess favorable attributes such as shape preservation [24] and degree reduction [25], which enable them to exhibit remarkable advantages in solving complex geometric and physical problems. In engineering applications, they are widely used in computer-aided design and can achieve precise modeling and analysis of structures. These properties endow them with great potential as excellent basis functions in the framework of the FEM. Goodman and Said [26] showed that the generalized Ball representation was superior to the Bézier representation for degree manipulation in polynomial curves and extended it to polynomial surfaces over triangles. In 1996, Hu et al. [27] designated the two types of generalized Ball curves, as established by Wang and Said, as Wang-Ball curves and Said-Ball curves, respectively. Zhang et al. [28] used inner product and conversion matrices to find explicit dual basis functions for Wang-Bézier type generalized Ball bases with respect to the Jacobi weight, including cases with and without boundary constraints. Hamza [29] proposed a new Wang-Ball curve degree approximation reduction algorithm that used the continuity of G^0, G^1, and G^2 to maintain the integrity of boundary control points and ensured geometric continuity at the boundaries.

In this paper, we use a new class of basis functions introduced above, namely the Wang-Ball basis functions, as the basis functions of the FEM to solve the Poisson equation with mixed boundary conditions in both 2D and 3D. This method uses the Wang-Ball basis functions to construct the trial and test function spaces, thereby obtaining the Galerkin formulation. Next, we give the definition of the Wang-Ball operator used to obtain the error estimates in terms of the H^1-semi norm, as well as the L^2 and L^∞ norms. In addition, the effectiveness of this method is illustrated through several numerical examples under different electrostatics backgrounds. With the use of high-degree Wang-Ball basis functions in these examples, the Runge-Kutta phenomenon does not occur, and the results are consistent with the error estimates.

The structure of this paper is as follows: In Section 2, we introduce some basic symbols. In Section 3, we present the definitions of Wang-Ball basis functions and Wang-Ball elements and provide the unisolvence of these elements. In Section 4, we construct the trial and test function spaces by utilizing Wang-Ball elements and present the Galerkin formulation of the FEM to solve the Poisson equation with mixed boundary conditions in 2D and 3D. In Section 5, we first give the definition of the Wang-Ball operator, then we derive the error estimate on H^1-semi, L^2, and L^∞ norms. In Section 6, several numerical examples under different electrostatics backgrounds are given to get the results. In Section 7, we summarize the entire work and describe some prospects for future work.

2. Preliminaries and notations

Let Ω be a bounded Lebesgue measurable polygon or polyhedron domain of the electrostatic field in $\mathbb{R}^n$ ($n = 2, 3$). The set of degree p integrable functions on Ω is called the L^p space

$$L^p(\Omega) = \{u : \|u\|_{L^p(\Omega)} < \infty\},$$

and the corresponding norm is defined as

$$\|u\|_{L^p(\Omega)} = \left(\int_\Omega |u(x)|^p \, dx\right)^{1/p}, \quad 1 \le p < \infty,$$
$$\|u\|_{L^\infty(\Omega)} = \text{ess sup}\{|u(x)| : \ x \in \Omega\}, \quad p = \infty.$$

The set of locally integrable functions is denoted by

$$L^p_{loc}(\Omega) = \{u : \ u \in L^p(K) \quad \forall \text{ compat } K \subset \text{interior } \Omega\}.$$

By using the definition of weak derivatives, the Lebesgue norm and space can be generalized.

Definition 2.1. *[30] Given a function $u(x) \in L^p_{loc}(\Omega)$, if a function $v(x) \in L^p_{loc}(\Omega)$ exists such that*

$$\int_\Omega v(x)\varphi(x)\, dx = (-1)^{|\alpha|} \int_\Omega u(x) D^\alpha \varphi(x)\, dx \quad \forall \varphi \in C_0^\infty(\Omega),$$

then $u(x)$ is called a weak derivative of $v(x)$, denoted as $D^\alpha u = v$.

We now provide the definition of the Sobolev space $W^m_p(\Omega)$ as follows:

$$W^m_p(\Omega) = \left\{u \in L^p_{loc}(\Omega) : \ \|u\|_{W^m_p(\Omega)} < \infty\right\}.$$

The corresponding norm is defined as

$$\|u\|_{W^m_p(\Omega)} = \left(\sum_{|\alpha| \le m} \|D^\alpha u\|^p_{L^p(\Omega)}\right)^{1/p}, \quad 1 \le p < \infty,$$
$$\|u\|_{W^m_\infty(\Omega)} = \max_{|\alpha| \le m} \|D^\alpha u\|_{L^\infty(\Omega)}, \qquad p = \infty.$$

In addition, the semi-norm is defined as

$$|u|_{W^m_p(\Omega)} = \left(\sum_{|\alpha| = m} \|D^\alpha u\|^p_{L^p(\Omega)}\right)^{1/p}, \quad 1 \le p < \infty,$$
$$|u|_{W^m_\infty(\Omega)} = \max_{|\alpha| = m} \|D^\alpha u\|_{L^\infty(\Omega)}, \qquad p = \infty.$$

When $p = 2$, we write $W^m_p(\Omega)$ as $H^m(\Omega)$ and $H^m_0(\Omega)$ is a subspace of $H^m(\Omega)$, consisting of functions that vanish on the boundary $\partial\Omega$.

3. Wang-Ball elements

In this section, we first introduce the definition of Wang-Ball basis functions and show their properties, such as positivity, symmetry, and endpoint. We then present the definition of Wang-Ball elements and also verify their unisolvence.

3.1. Wang-Ball basis functions

Definition 3.1. *[27] The degree m Wang-Ball basis functions are defined for both odd and even values in* $[0, 1]$ *as follows:*

$$A_i^m(x) = \begin{cases} (2x)^i(1-x)^{i+2}, & 0 \le i \le \left\lfloor \frac{m}{2} \right\rfloor - 1, \\ (2x)^{\lfloor m/2 \rfloor}(1-x)^{\lceil m/2 \rceil}, & i = \left\lfloor \frac{m}{2} \right\rfloor, \\ (2(1-x))^{\lfloor m/2 \rfloor}x^{\lceil m/2 \rceil}, & i = \left\lceil \frac{m}{2} \right\rceil, \\ A_{m-i}^m(1-x), & \left\lceil \frac{m}{2} \right\rceil + 1 \le i \le m, \end{cases} \tag{3.1}$$

where i represents the index of the Wang-Ball basis function, $\lfloor \frac{m}{2} \rfloor$ *represents the maximum integer less than or equal to* $\frac{m}{2}$*, and* $\lceil \frac{m}{2} \rceil$ *represents the minimum integer greater than or equal to* $\frac{m}{2}$*.*

When $m = 3$ and 5, we can respectively obtain 3- and 5-degree Wang-Ball basis functions (see Figure 1).

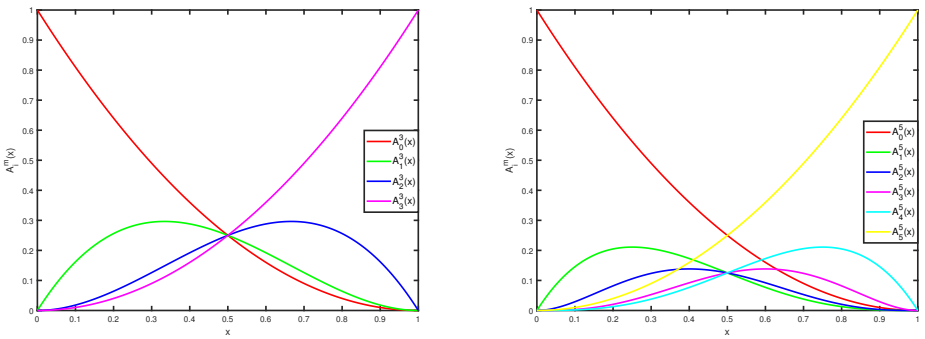

(a) 3-degree Wang-Ball basis functions (b) 5-degree Wang-Ball basis functions

Figure 1. Three- and five-degree Wang-Ball basis functions.

Below, we present some properties of the functions.

Property 3.1. *[26] Wang-Ball basis functions have the following properties:*

(1) Positivity: $0 \le A_i^m(x) \le 1$, $0 \le x \le 1$, $i = 0, 1, \cdots, m$.

(2) Partition of unity: $\sum_{i=0}^{m} A_i^m(x) = 1$, $0 \le x \le 1$.

(3) Symmetry: $A_i^m(x) = A_{m-i}^m(1-x)$, $i = 0, 1, \cdots, m$.

(4) Recursion: Let $F(x) = 2(1-x)x$*, then*

$$\begin{cases} A_i^m(x) = A_i^{m-1}(x) = (1-x)^2 F^i(x), & 0 \le i \le \lceil m/2 \rceil - 2, \\ A_i^m(x) = A_{i-1}^{m-1}(x) = x^2 F^{m-i}(x), & \lfloor m/2 \rfloor + 2 \le i \le m, \\ A_{\lceil m/2 \rceil - 1}^m(x) = (1-x) A_{\lceil m/2 \rceil - 1}^{m-1}(x), \\ A_{\lfloor m/2 \rfloor + 1}^m(x) = x A_{\lfloor m/2 \rfloor}^{m-1}(x), \\ A_m^{2m}(x) = x A_{m-1}^{2m-1}(x) + (1-x) A_m^{2m-1}(x), \\ A_{i+1}^{m+2}(x) = A_i^m(x) F(x), & 0 \le i \le m. \end{cases}$$

(5) *Linear independence: These basis function are linearly independent.*

(6) *Endpoint property: At the endpoints* $x = 0$ *and* $x = 1$*, there is only one Wang-Ball basis function with a value of* 1*, and all others are* 0*, that is*

$$A_i^m(0) = \begin{cases} 1, & i = 0, \\ 0, & i \neq 0, \end{cases} \qquad A_i^m(1) = \begin{cases} 1, & i = m, \\ 0, & i \neq m. \end{cases}$$

Definition 3.2. *Given the control points* $\boldsymbol{P}_i \in \mathbb{R}^3$ $(i = 0, 1, \cdots, m)$*, the Wang-Ball curve of degree* m *is expressed as follows:*

$$\boldsymbol{W}(x) = \sum_{i=0}^{m} \boldsymbol{P}_i A_i^m(x), \quad x \in [0, 1], \tag{3.2}$$

where $A_i^m(x)$ *are the Wang-Ball basis functions defined above.*

When $m = 3$ and 5, we can obtain 3- and 5-degree Wang-Ball curves, respectively (see Figure 2).

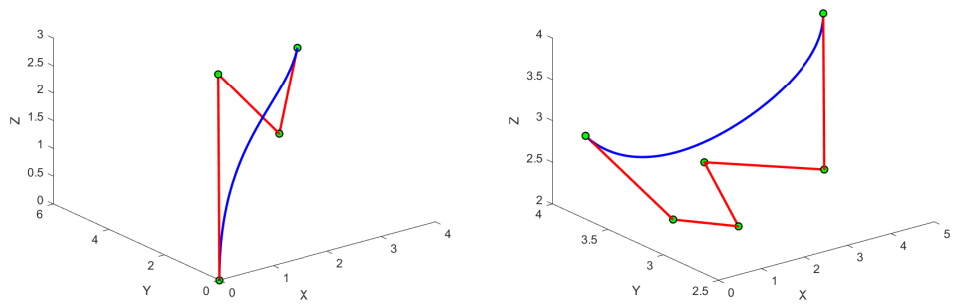

(a) 3-degree Wang-Ball curve (b) 5-degree Wang-Ball curve

Figure 2. Three- and five-degree Wang-Ball curves.

The Wang-Ball curve has the following endpoint interpolation property:

$$\boldsymbol{W}(0) = \boldsymbol{P}_0, \quad \boldsymbol{W}(1) = \boldsymbol{P}_m.$$

Consequently, the 2D $m \times n$-degree tensor product Wang-Ball basis functions are represented by the following expression:

$$A_{i,j}^{m,n}(x, y) = A_i^m(x) A_j^n(y),$$

and the 3D $m \times n \times t$-degree tensor product Wang-Ball basis functions are

$$A_{i,j,l}^{m,n,t}(x, y, z) = A_i^m(x) A_j^n(y) A_l^t(z),$$

where $A_i^m(x)$, $A_j^n(y)$ and $A_l^t(z)$ $(i = 0, 1, \cdots, m, j = 0, 1, \cdots, n, l = 0, 1, \cdots, t)$ are all Wang-Ball basis functions defined above. We now give the definition of the Wang-Ball surface in 2D and the situation in 3D is similar.

Definition 3.3. *Given control points* $\boldsymbol{P}_{i,j} \in \mathbb{R}^3$ $(i = 0, 1, \cdots, m, j = 0, 1, \cdots, n)$*, the Wang-Ball surface of degree* $m \times n$ *is expressed as follows:*

$$\boldsymbol{W}(x, y) = \sum_{i=0}^{m} \sum_{j=0}^{n} \boldsymbol{P}_{i,j} A_{i,j}^{m,n}(x, y), \quad (x, y) \in [0, 1] \times [0, 1], \tag{3.3}$$

where $A_{i,j}^{m,n}(x, y)$ $(i = 0, 1, \cdots, m, j = 0, 1, \cdots, n)$ *is the* $m \times n$*-degree tensor product Wang-Ball basis functions defined above.*

We can also obtain 3×3- and 5×5-degree Wang-Ball surfaces, respectively (see Figure 3).

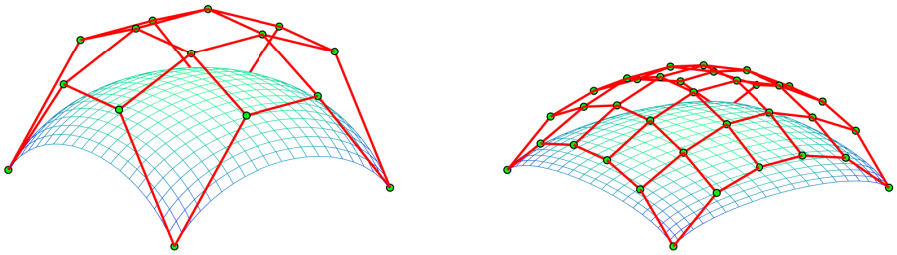

(a) 3×3-degree Wang-Ball surface (b) 5×5-degree Wang-Ball surface

Figure 3. The 3×3- and 5×5-degree Wang-Ball surfaces.

The Wang-Ball surface has the following corner interpolation property:

$$\boldsymbol{W}(0, 0) = \boldsymbol{P}_{0,0},\ \boldsymbol{W}(0, 1) = \boldsymbol{P}_{0,n},\ \boldsymbol{W}(1, 0) = \boldsymbol{P}_{m,0},\ \boldsymbol{W}(1, 1) = \boldsymbol{P}_{m,n}.$$

3.2. Wang-Ball elements

In this subsection, we first give the definition of Wang-Ball elements based on the Wang-Ball basis functions defined in the previous subsection, and then we discuss their unisolvence.

A finite element $(E, \mathcal{P}, \mathcal{N})$ is defined by Ciarlet [31] as follows:

Definition 3.4. *Let the following hold*

- E *is a element.*
- $\mathcal{P}$ *is the shape function space.*
- $\mathcal{N} = \{N_1, N_2, \cdots, N_k\}$ *is the degrees of freedom (DoFs).*

Then $(E, \mathcal{P}, \mathcal{N})$ *is a finite element.*

First, let us introduce two lemmas that will be used later.

Lemma 3.1. *[30] Let* P *be a polynomial of degree* $k \geq 1$ *that vanishes on a hyperplane* L*. Then we can write* $P = LQ$*, where* Q *is a polynomial of degree* $k - 1$*.*

Lemma 3.2. *[30] Let* $\mathcal{P}$ *be a* k*-D space and let* $\{N_1, N_2, \cdots, N_k\}$ *be a subset of* $\mathcal{P}'$*. Then the following two statements are equivalent:*

(a) $\{N_1, N_2, \cdots, N_k\}$ *is a basis for* $\mathcal{P}'$.
(b) Given $v \in \mathcal{P}$ *with* $N_i v = 0$*, then* $v \equiv 0$*, where* $i = 1, 2, \cdots, k$.

According to Lemma 3.2, it can be concluded that each function within the shape function space can be uniquely expressed through its DoF values. Next, we present the definition of Wang-Ball elements and illustrate their unisolvence through a theorem.

Let Ω_h be a subdivision of the electrostatic field domain Ω introduced in Section 2, consisting of a rectangular element in $\mathbb{R}^2$ or a cuboid element in $\mathbb{R}^3$. For every element $E \in \Omega_h$, h_E is the diameter of E and B_E is the largest ball contained in E with the diameter ρ_E. We say that Ω_h is regular satisfying the requirement that a constant $\sigma > 1$ exists such that for all $E \in \Omega_h$,

$$\rho_E \geq \sigma h_E. \tag{3.4}$$

We also set the mesh size h of Ω_h by using

$$h = \max_{E \in \Omega_h} h_E.$$

As depicted in Figure 4(*a*), E is a rectangular element in $\mathbb{R}^2$ and $A^{m,n}_{i,j}(x, y)$, $A^{m,n}_{i+1,j}(x, y)$, $A^{m,n}_{i,j+1}(x, y)$, and $A^{m,n}_{i+1,j+1}(x, y)$ around E are the $m \times n$-degree tensor product Wang-Ball basis functions defined above. There are also similar $m \times n \times t$-degree tensor product Wang-Ball basis functions for the cuboid element E in $\mathbb{R}^3$ as shown in Figure 4(*b*).

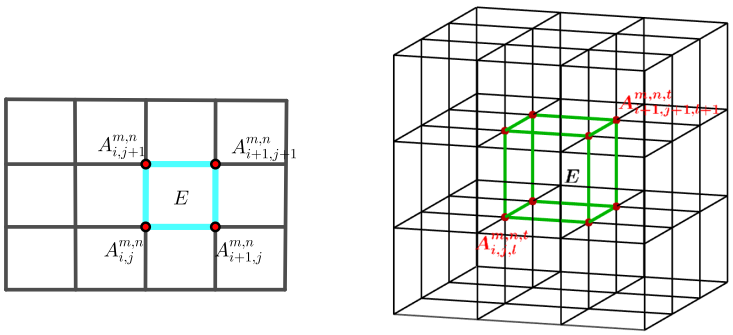

(a) Part of the rectangular subdivision (b) Part of the cuboid subdivision

Figure 4. Subdivision.

Similar to Definition 3.4, we provide the definition of Wang-Ball elements.

Definition 3.5. *For* $\mathbb{R}^n$ $(n = 2, 3)$*, we say that* $(E, \mathcal{P}, \mathcal{N})$ *is a Wang-Ball element if it satisfies the following.*

- *E is a rectangular or cuboid element.*
- *For* $\mathbb{R}^2$,

$$\mathcal{P} = span\left\{A^{m,n}_{i,j}(x, y), A^{m,n}_{i+1,j}(x, y), A^{m,n}_{i,j+1}(x, y), A^{m,n}_{i+1,j+1}(x, y)\right\},$$

or for $\mathbb{R}^3$,

$$\mathcal{P} = span\Big\{A^{m,n,t}_{i,j,l}(x,y,z), A^{m,n,t}_{i+1,j,l}(x,y,z), A^{m,n,t}_{i,j+1,l}(x,y,z),$$
$$A^{m,n,t}_{i+1,j+1,l}(x,y,z), A^{m,n,t}_{i,j,l+1}(x,y,z), A^{m,n,t}_{i+1,j,l+1}(x,y,z),$$
$$A^{m,n,t}_{i,j+1,l+1}(x,y,z), A^{m,n,t}_{i+1,j+1,l+1}(x,y,z)\Big\}.$$

- $\mathcal{N} = \left\{N_{i,j}\right\}\left(\left\{N_{i,j,l}\right\}\right)$ *is the degrees of freedom (DoFs), satisfying* $N_{i,j}v = v\left(\boldsymbol{P}_{i,j}\right)\left(N_{i,j,l}v = v\left(\boldsymbol{P}_{i,j,l}\right)\right)$, *where* $\boldsymbol{P}_{i,j}\left(\boldsymbol{P}_{i,j,l}\right)$ *is the control vertices of the* $m \times n$ $(m \times n \times t)$*-degree Wang-Ball surface and* $i = 0, 1, \cdots, m,\ j = 0, 1, \cdots, n,\ l = 0, 1, \cdots, t$.

Theorem 3.1. *If* $(E, \mathcal{P}, \mathcal{N})$ *is a Wang-Ball element, then* $\mathcal{N} = \left\{N_{i,j}\right\}\left(\left\{N_{i,j,l}\right\}\right)$ *is a basis of* $\mathcal{P}'$, *where* $i,\ j,\ l = 0, 1, \cdots, k$.

Proof. We only consider the case for $\mathbb{R}^2$; the case of $\mathbb{R}^3$ is similar. Let E be an element in the rectangular subdivision Ω_h. We then define

$$V_h = \left\{v \in H^1(\Omega) : v|_E \in Q_k,\ E \in \Omega_h\right\},$$

where Q_k denotes the set of $k \times k$-degree tensor product Wang-Ball basis functions.

Let $\mathcal{P} = Q_k$ and $\mathcal{N}$ denote the evaluations of the control vertices $\boldsymbol{P}_{i,j}\,(i, j = 0, 1, \cdots, k)$. For simplicity, we denote the control vertices as $\left\{(x_i, y_j) :\ i, j = 0, 1, \cdots, k\right\}$ as depicted in Figure 5.

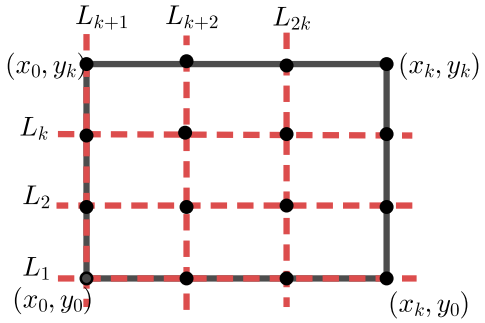

Figure 5. Rectangle of $k \times k$-degree Wang-Ball basis functions.

One can show that the number of degrees of freedom $\mathcal{N}$ is $(k+1)^2$ and

$$dim\,\mathcal{P} = dim\,Q_k = (k+1)^2,$$

so $\mathcal{N}$ is equal to $dim\,\mathcal{P}$.

Suppose that the polynomial $v \in Q_k$ takes the value of zero at all points shown in Figure 5. When v is restricted to any side of the rectangle, the resulting function is a polynomial of degree k in one variable. We rewrite $v = c\prod_{i=1}^{2k} L_i$ by using Lemma 3.1, where c is a constant. However,

$$0 = v(x_k, y_k) = c\prod_{i=1}^{2k} L_i(x_k, y_k) \Longrightarrow c = 0,$$

since $L_i(x_k, y_k) \neq 0$ for $i = 1, 2, \cdots, 2k$. Thus, $v \equiv 0$. Then, by Lemma 3.2, $\mathcal{N} = \left\{N_{i,j} : i,\ j = 0, 1, \cdots, k\right\}$ is a basis of $\mathcal{P}'$. □

In this section, we give the definition of Wang-Ball elements based on the Wang-Ball basis functions and prove their unisolvence. In the next section, we show how to use them to solve the Poisson equation.

4. The FEM with Wang-Ball elements

The expression of the Poisson equation in the electrostatic field in Ω with with the boundary $\partial\Omega = \Gamma_N \cup \Gamma_D$ is

$$-\nabla^2\Phi = \frac{\rho}{\varepsilon_0}, \qquad \text{in } \Omega, \tag{4.1a}$$

$$\nabla\Phi \cdot \boldsymbol{n} = p, \qquad \text{on } \Gamma_N, \tag{4.1b}$$

$$\Phi = g, \qquad \text{on } \Gamma_D, \tag{4.1c}$$

where Φ is the electric potential, ρ is the charge density, ε_0 is the permittivity of free space, $\boldsymbol{n}$ is the outward normal unit vector, Γ_N is the Neumann boundary, and Γ_D is the Dirichet boundary with $\Gamma_N \cap \Gamma_D = \varnothing$.

For simplicity, in the following text, we use f instead of $\frac{\rho}{\varepsilon_0}$ in Eq (4.1).

Remark 4.1. *The mixed boundary conditions mean that the Dirichlet boundary condition (specifying the value of the electric potential Φ) and the Neumann boundary condition (specifying the value of the normal derivative of the electric potential Φ) exist simultaneously in different parts of the solution region.*

The Dirichlet boundary condition that specifies the value of the electric potential usually corresponds to the surface of a conductor with a known electric potential. This indicates that on the boundary, the electric potential is fixed at a definite value, which reflects the property of the conductor as an equipotential body. The Neumann boundary condition specifies the normal derivative of the electric potential. When $\nabla\Phi \cdot \boldsymbol{n} = p$ is specified, it means that the electric flux passing through a unit area on the boundary is known.

By multiplying the test function $v \in H_0^1(\Omega)$ on both sides of Eq (4.1a), we obtain

$$\int_\Omega -\nabla^2\Phi v \, d\Omega = \int_\Omega f v \, d\Omega.$$

Using the Green formula and divergence theorem, yields

$$\int_\Omega \nabla\Phi \cdot \nabla v \, d\Omega - \int_{\Gamma_N} pv \, ds = \int_\Omega f v \, d\Omega.$$

For simplicity, we define

$$a(\Phi, v) = \int_\Omega \nabla\Phi \cdot \nabla v \, d\Omega, \tag{4.2}$$

$$(f, v) = \int_\Omega f v \, d\Omega + \int_{\Gamma_N} pv \, ds. \tag{4.3}$$

In summary, it can be known that the variational formulation of the Poisson equation is to find $\Phi \in H^1(\Omega)$ satisfying

$$a(\Phi, v) = (f, v) \qquad \forall v \in H_0^1(\Omega). \tag{4.4}$$

In addition, we also say that Φ satisfies the regularity assumption, that is, a constant C exists such that

$$\|\Phi\|_{W_2^2(\Omega)} \leq C\|f\|_{L^2(\Omega)}. \tag{4.5}$$

Next, we will construct the Wang-Ball element spaces in $\mathbb{R}^n\,(n = 2, 3)$. Here Ω_h represents the uniformly divided elements shown in Figure 4 in Section 3. The Wang-Ball element basis function spaces are the shape function space $\mathcal{P}$ defined in Definition 3.5.

For every Wang-Ball element node $x_j\,(j = 1, \cdots, N_b)$, we define the associated Wang-Ball element basis function ξ_j in such a manner that $\xi_j|_{\Omega_h} \in \mathcal{P}$, where $j = 1, \cdots, N_b$. For the rectangular or cuboid element E, we give the definition of the finite dimensional subspace U_h for Φ as follows:

$$U_h = \left\{\Phi \in H^1(\Omega) : \Phi|_E \in \mathcal{P},\ E \in \Omega_h\right\}.$$

Let $U_{h_0} = \{v \in U_h : v\,|_{\partial\Omega} = 0\}$. By choosing the test function $v \in U_{h_0}$, we obtain the following Galerkin formulation.

Galerkin formulation. A numerical approximation for Eq (4.1) in $\mathbb{R}^n\,(n = 2, 3)$ can be obtained by finding $\Phi_h \in U_h$ satisfying the boundary condition (4.1b) and (4.1c) [32] such that

$$a(\Phi_h, v) = (f, v) \qquad \forall v \in U_{h_0}. \tag{4.6}$$

The results of this section indicate that we have found a FEM with Wang-Ball elements that can derive the Galerkin formulation in 2D and 3D. Therefore, in the next section, we provide an error analysis.

5. Error analysis

In the previous section, we derived the Galerkin formulation of the FEM with Wang-Ball elements. In this section, we analyze its error. We introduce an operator used for error estimation.

5.1. The Wang-Ball operator

Let $(E, \mathcal{P}, \mathcal{N})$ be a Wang-Ball element. For simplicity, we use A_i to represent the tensor product Wang-Ball basis functions of degree k on each variable in $\mathcal{P}$, and use N_i to represent the control vertices in $\mathcal{N}$, where $i = 1, 2, \cdots, (k+1)^n$ for $\mathbb{R}^n\,(n = 2, 3)$. In addition, we use $x_i\,(i = 1, 2, \cdots, (k+1)^n)$ to represent each control vertex.

First, let $\overline{E}$ be the closure of E. Both $\mathcal{P}$ and $\mathcal{N}$ are defined in Definition 3.5, and thus we can get the definition of the Wang-Ball operator.

If Φ is a function that defines all control vertices in $\mathcal{N}$, then we define the local Wang-Ball operator $\mathscr{A}_E : C^l(\overline{E}) \to \mathcal{P}$ in E as

$$\mathscr{A}_E\Phi = \sum_{i=1}^{(k+1)^n} N_i(\Phi)A_i. \tag{5.1}$$

According to the definition of the Wang-Ball basis functions, we can directly conclude that the Wang-Ball operator $\mathscr{A}_E$ is linear. One very important property of the Wang-Ball operator is local polynomial reproduction. Introducing this property simplifies the error analysis.

Property 5.1. *$\mathscr{A}_E f_k = f_k$ for $f_k \in \mathcal{P}$.*

Proof. Since the Wang-Ball basis functions are linearly independent according to Property 3.1, for $f_k \in \mathcal{P}$, we have

$$f_k = \sum_{i=1}^{(k+1)^n} a_i A_i, \tag{5.2}$$

where a_i represents the coefficients.

When $k = 0$, i.e., $f = a$, by Eq (5.1) and the partition of unity of Property 3.1, we obtain

$$\mathscr{A}_E f_k = \sum_{i=1}^{(k+1)^n} f_k(x_i)\, A_i = a \sum_{i=1}^{(k+1)^n} A_i = a,$$

and thus $\mathscr{A}_E f_k = f_k$.

Assuming that when $k = m - 1$ for $2 \le m \le k$, $\mathscr{A}_E f_k = f_k$ holds.

When $k = m$, by the recursion of Property 3.1, we only prove the case when $i = \lfloor m/2 \rfloor$, and the other cases can be deduced similarly. For ease of identification in this proof process, we use A_{i_k} to represent the tensor product Wang-Ball basis functions of degree k on each variable in $\mathbb{R}^n$ ($n = 2, 3$). Thus, we have

$$\mathscr{A}_E f_k = f_k(x_i) A_{i_k} = f_k(x_i) x^n A_{i_{k-1}} = x^n f_k(x_i) A_{i_{k-1}} = x^n f_{k-1} = f_k,$$

where the fourth equation holds because $f_k(x_i)$ represents the coefficient a_i of Eq (5.2).

So for $f_k \in \mathcal{P}$, we prove that $\mathscr{A}_E f_k = f_k$. □

We then show that the operator $\mathscr{A}_E$ is bounded through the following lemma.

Lemma 5.1. *Let $(E, \mathcal{P}, \mathcal{N})$ be a Wang-Ball element with $h_E = 1$, $\mathcal{P} \subseteq W_\infty^m(E)$, and $\mathcal{N} \subseteq (C^l(\overline{E}))'$. Then the Wang-Ball operator $\mathscr{A}_E$ is bounded from $C^l(\overline{E})$ to $W_p^m(E)$, that is*

$$\|\mathscr{A}_E \Phi\|_{W_p^m(E)} \le C \|\Phi\|_{C^l(\overline{E})}. \tag{5.3}$$

Proof. The Wang-Ball operator is defined by $\mathscr{A}_E \Phi = \sum_{i=1}^{(k+1)^n} N_i(\Phi) A_i^k$ and we know each $A_i \in W_\infty^m(E) \subseteq W_p^m(E)$. Then

$$\begin{aligned}
\|\mathscr{A}_E \Phi\|_{W_p^m(E)} &\le \sum_{i=1}^{(k+1)^n} |N_i(\Phi)| \|A_i\|_{W_p^m(E)} \\
&\le \left(\sum_{i=1}^{(k+1)^n} \|N_i\|_{(C^l(\overline{E}))'} \|A_i\|_{W_p^m(E)} \right) \|\Phi\|_{C^l(\overline{E})} \\
&\le C \|\Phi\|_{C^l(\overline{E})}.
\end{aligned}$$

□

Now, we give the definition of affine equivalence. Let $(\hat{E}, \hat{\mathcal{P}}, \hat{\mathcal{N}})$ be the reference element and let $F\hat{x} = a\hat{x} + b$ be an affine map. $(E, \mathcal{P}, \mathcal{N})$, as defined in Definition 3.5, is the affine equivalent to $(\hat{E}, \hat{\mathcal{P}}, \hat{\mathcal{N}})$ if the following hold.

(a) $F(\hat{E}) = E$.
(b) $F^*\mathcal{P} = \hat{\mathcal{P}}$, where the pull-back F^* is defined by $F^*(f) := f \circ F$.
(c) $F_*\hat{\mathcal{N}} = \mathcal{N}$, where the push-forward F_* is defined by $(F_*N)(f) := N(F^*(f))$.

Let $\varrho(E)$ be the operator norm of the Wang-Ball operator $\mathscr{A}_E$. Since E ranges over a collection of elements, we now investigate the dependence of $\varrho(\hat{E})$ on affine transformations for future use.

Lemma 5.2. *Given a reference element* $(\hat{E}, \hat{\mathcal{P}}, \hat{\mathcal{N}})$ *and an affine-equivalent element* $(E, \mathcal{P}, \mathcal{N})$ *with the affine map* $F\hat{x} = a\hat{x} + b$, *we have*

$$\varrho(E) \leq C\,\chi(a),$$

where C *is a constant and* χ *is a continuous function on* $GL(\mathbb{R}^n)$.

Proof. Let the reference element $(\hat{E}, \hat{\mathcal{P}}, \hat{\mathcal{N}})$ be affine equivalent to $(E, \mathcal{P}, \mathcal{N})$ through the affine map $F\hat{x} = a\hat{x} + b$, $a = (a_{ij})$ and let the inverse of a be $(a^{-1})_{ij}$. According to the definition of affine equivalence, we have

$$\mathscr{A}\Phi(x) = \sum_{i=1}^{(k+1)^n} (F_*N_i)\Phi \cdot (F^{-1})^* A_i(x).$$

Since $(F_*N_i)\Phi = N_i(F^*\Phi)$ for $i = 1, 2, \cdots, (k+1)^n$ and $(F^*\Phi)\hat{x} = \Phi(F\hat{x})$, we get

$$|(F_*N_i)\,\Phi| = |N_i\,(F^*\Phi)| \leq C\,\|F^*\Phi\|_{C^l\left(\overline{\hat{E}}\right)} \leq C\left(1 + \max_{1\leq i,j\leq n}\left|a_{ij}\right|\right)^l \|\Phi\|_{C^l(\overline{E})},$$

and

$$\left\|\left(F^{-1}\right)^* A_i\right\|_{W_p^{k+1}(E)} \leq C'\left(1 + \max_{1\leq i,j\leq n}\left|\left(a^{-1}\right)_{ij}\right|\right)^{k+1} \|A_i\|_{W_p^{k+1}(\hat{E})}\,|\det a|^{1/p}.$$

Since $\|A_i\|_{W_p^{k+1}(\hat{E})}$ is bounded, we have

$$\|\mathscr{A}\Phi\|_{W_p^{k+1}(E)} \leq C\left(1 + \max_{1\leq i,j\leq n}\left|a_{ij}\right|\right)^l \left(1 + \max_{1\leq i,j\leq n}\left|\left(a^{-1}\right)_{ij}\right|\right)^{k+1} |\det a|^{1/p}\|\Phi\|_{C^l(\overline{E})}.$$

Therefore,

$$\varrho(E) \leq C\left(1 + \max_{1\leq i,j\leq n}\left|a_{ij}\right|\right)^l \left(1 + \max_{1\leq i,j\leq n}\left|\left(a^{-1}\right)_{ij}\right|\right)^{k+1} |\det a|^{1/p}.$$

When we take $\chi(a) = \left(1 + \max_{1\leq i,j\leq n}\left|a_{ij}\right|\right)^l \left(1 + \max_{1\leq i,j\leq n}\left|\left(a^{-1}\right)_{ij}\right|\right)^{k+1} |\det a|^{1/p}$, this lemma has been proven. □

Next, we give the definition of the global Wang-Ball operator $\mathscr{A}_h$ in Ω as follows:

$$\mathscr{A}_h\Phi|_E = \mathscr{A}_E\Phi, \quad \text{for all } E \in \Omega_h.$$

Similar to Lemma 5.1, we can also prove that this global Wang-Ball operator $\mathscr{A}_h$ is bounded.

In this subsection, we give the definition of the Wang-Ball operator, and we will use it for error estimates in the next subsections.

5.2. Error estimates in the H^1-semi norm

In this subsection, we derive error estimates in the H^1-semi norm. To begin with, we give the definition of an averaged version of the Taylor polynomial.

Definition 5.1. *Assume that the function Φ has weak derivatives whose orders are strictly lower than m within Ω such that $B \subset\subset \Omega$. Then the Taylor polynomial of order m of Φ, which is averaged over B, is defined in the following way:*

$$Q^m\Phi(x) = \int_B \sum_{|\alpha|<m} \frac{1}{\alpha!} D^\alpha \Phi(y)(x-y)^\alpha \phi(y) dy, \tag{5.4}$$

where $\alpha = (\alpha_1, \alpha_2, \cdots, \alpha_n)$ is an n-tuple of non-negative integers, B is the ball with x_0 as the center and ρ as the radius, and ϕ is the cut-off function supported in $\overline{B}$.

We then provide the definition of C^r elements with $r \geq 0$. If $\mathscr{A}_E f \in C^r(\Omega)$ for all $f \in C^m(\Omega)$, then we say that $\mathscr{A}_E f$ has continuity of order r (i.e., C^r) and $V_{\mathscr{A}} = \{\mathscr{A}_E f : f \in C^m(\Omega)\}$ is the C^r space. Then the Wang-Ball elements which can be used to construct the C^r spaces are called C^r elements.

Before deriving the error estimates in the H^1-semi norm for the solution Φ and Φ_h in Eqs (4.1) and (4.6), respectively, we derive the error estimates of the solution Φ and $\mathscr{A}_h\Phi$ of the Wang-Ball operator.

Theorem 5.1. *Let Ω_h be a family of subdivisions of Ω in $\mathbb{R}^n$ and $(E, \mathcal{P}, \mathcal{N})$ be a C^r Wang-Ball element. Then a constant $C > 0$ independent of h exists such that, for any $\Phi \in H^{k+1}(\Omega)$ and $0 \leq s \leq \min\{k+1, r+1\}$, we have*

$$|\Phi - \mathscr{A}_h\Phi|_{H^s(\Omega)} \leq C\, h^{k+1-s}\, |\Phi|_{H^{k+1}(\Omega)}, \tag{5.5}$$

where $\mathscr{A}_h\Phi \in U_h$.

Proof. To derive the inequality (5.5) in the domain Ω, we firstly derive an error estimate in a single element E for $0 \leq s \leq k+1$ and $\Phi \in H^{k+1}(E)$ as follows:

$$|\Phi - \mathscr{A}_E\Phi|_{H^s(E)} \leq C\, h_E^{k+1-s} |\Phi|_{H^{k+1}(E)}, \tag{5.6}$$

where $C = C_{k,n,\gamma,\varrho(\hat{E})}$, $\hat{E} = \{(1/\mathrm{diam}E)x : x \in E\}$, and $\varrho(\hat{E})$ is the operator norm introduced by Lemma 5.1.

For the derivation of inequality (5.6), it is sufficient to take $h_E = 1\,(diam\, E = diam\, \hat{E})$, and the general case can then be obtained through a homogeneity argument; B_E and $Q^{k+1}\Phi$ are both as defined above.

Since the Wang-Ball operator $\mathscr{A}_E$ is local polynomial reproduction, that is, $\mathscr{A}_E f = f$ for $f \in \mathcal{P}$ and $Q^{k+1}\Phi \in \mathcal{P}$, we have

$$\mathscr{A}_E Q^{k+1}\Phi = Q^{k+1}\Phi.$$

Thus, we use the Bramble-Hilbert lemma [30], that is, a constant $C > 0$ exists such that

$$|\Phi - Q^{k+1}\Phi|_{H^s(E)} \leq C d^{k+1-s} |\Phi|_{H^{k+1}(E)}, \quad s = 0, 1, \cdots, k+1. \tag{5.7}$$

We then have

$$\begin{aligned}|\Phi - \mathscr{A}_E\Phi|_{H^{k+1}(E)} &\le |\Phi - Q^{k+1}\Phi|_{H^{k+1}(E)} + |Q^{k+1}\Phi - \mathscr{A}_E\Phi|_{H^{k+1}(E)}\\ &= |\Phi - Q^{k+1}\Phi|_{H^{k+1}(E)} + |\mathscr{A}_E(Q^{k+1}\Phi - \Phi)|_{H^{k+1}(E)}\\ &\le |\Phi - Q^{k+1}\Phi|_{H^{k+1}(E)} + \varrho(E)|Q^{k+1}\Phi - \Phi|_{C^l(\overline{E})}\\ &\le (1 + \varrho(E)C)\,|\Phi - Q^{k+1}\Phi|_{H^{k+1}(E)}\\ &\le (1 + \varrho(E)C)\,C\,|\Phi|_{H^{k+1}(E)}\\ &= C\,|\Phi|_{H^{k+1}(E)},\end{aligned}$$

where the positive contant C in these inequalities has different meanings with the last constant $C = C_{k,n,\gamma,\varrho(E)}$.

Next, we derive the inequality (5.5). First, we can find a unified boundary for $C_{k,n,\gamma,\varrho(\hat{E})}$ by Lemma 5.2. Since $\mathscr{A}_h\Phi|_E = \mathscr{A}_E\Phi$ and $h_E \le h$, for $0 \le s \le k+1$, we get

$$\begin{aligned}\left(\sum_{E\in\Omega_h} |\Phi - \mathscr{A}_E\Phi|^2_{H^s(E)}\right)^{1/2} &\le C\,h^{k+1-s}\left(\sum_{E\in\Omega_h} |\Phi|^2_{H^{k+1}(E)}\right)^{1/2}\\ &= C\,h^{k+1-s}\,|\Phi|_{H^{k+1}(\Omega)}.\end{aligned}$$

In addition, since the elements in the result above can form C^r elements for some $r \ge 0$, we have the following for $0 \le s \le r+1$:

$$\sum_{E\in\Omega_h} |\Phi - \mathscr{A}_E\Phi|^2_{H^s(E)} = |\Phi - \mathscr{A}_h\Phi|^2_{H^s(\Omega)}.$$

By substituting this expression on the left-hand side of the inequality above, we can prove inequality (5.5), where $0 \le s \le \min\{k+1,\ r+1\}$. □

According to the conclusion above, we can derive the error estimate in the H^1-semi norm for the solutions Φ and Φ_h in Eq (4.1) and the Galerkin formulation (4.6), respectively.

Theorem 5.2. *Let Φ_h be the solution of the Galerkin formulation (4.6). Assume that the exact solution of Eq (4.1) satisfies $\Phi \in H^2(\Omega)$. Then a constant $C > 0$ independent of h exists such that*

$$|\Phi - \Phi_h|_{H^1(\Omega)} \le C\,h^k\,|\Phi|_{H^{k+1}(\Omega)}.$$

Proof. Since Φ is the solution of the variational formulation (4.4) and Φ_h is the solution of the Galerkin formulation (4.6), we get the Galerkin orthogonality, that is,

$$a(\Phi - \Phi_h,\ v) = 0, \qquad \forall \Phi \in U_{h_0},$$

and by combining Schwarz's inequality [31], we have

$$|a(\Phi, v)| \le |\Phi|_{H^1(\Omega)}\,|v|_{H^1(\Omega)}, \qquad \forall \Phi, v \in H^1(\Omega),$$

we have

$$\begin{aligned}|\Phi - \Phi_h|^2_{H^1(\Omega)} &= a(\Phi - \Phi_h, \Phi - \Phi_h)\\ &= a(\Phi - \Phi_h, \Phi - v_h) + a(\Phi - \Phi_h, v_h - \Phi_h)\\ &= a(\Phi - \Phi_h, \Phi - v_h)\\ &\le |\Phi - \Phi_h|_{H^1(\Omega)}\,|\Phi - v_h|_{H^1(\Omega)}.\end{aligned}$$

If $|\Phi - \Phi_h|_{H^1(\Omega)} \neq 0$, we directly get

$$|\Phi - \Phi_h|_{H^1(\Omega)} \leq |\Phi - v_h|_{H^1(\Omega)}, \qquad \forall v_h \in U_{h_0}.$$

If $|\Phi - \Phi_h|_{H^1(\Omega)} = 0$, this inequality holds trivially. Thus,

$$|\Phi - \Phi_h|_{H^1(\Omega)} \leq C \inf_{v_h \in U_h} |\Phi - v_h|_{H^1(\Omega)}.$$

Taking Theorem 5.1 with $s = 1$, yields

$$\begin{aligned} |\Phi - \Phi_h|_{H^1(\Omega)} &\leq C \inf_{v_h \in U_h} |\Phi - v_h|_{H^1(\Omega)} \\ &\leq C\, |\Phi - \mathscr{A}_h \Phi|_{H^1(\Omega)} \\ &\leq C\, h^k\, |\Phi|_{H^{k+1}(\Omega)}. \end{aligned}$$

□

5.3. Error estimates in the L^2 norm

We will use a duality argument to derive the estimate in the L^2 norm from the estimate in the H^1-semi norm.

First, we give the dual equation of the Poisson equation which find that z satisfies

$$-\nabla^2 z = \Phi - \Phi_h, \quad \text{in } \Omega. \tag{5.8}$$

And according to the inequality (4.5), the regularity of this dual equations implies that a constant C exists such that

$$|z|_{H^2(\Omega)} \leq C\, \|\Phi - \Phi_h\|_{L^2(\Omega)}.$$

Theorem 5.3. *Let Φ_h be the solution of the Galerkin formulation (4.6). Assume that the exact solution of Eq (4.1) satisfies $\Phi \in H^2(\Omega)$. A constant $C > 0$ independent of h exists such that,*

$$\|\Phi - \Phi_h\|_{L^2(\Omega)} \leq C\, h^{k+1}\, |\Phi|_{H^{k+1}(\Omega)}.$$

Proof. Since $\Phi - \Phi_h \in L^2(\Omega)$, $z \in H^{k+1}(\Omega)$ for the dual equation (5.8), then

$$\|\Phi - \Phi_h\|^2_{L^2(\Omega)} = (\Phi - \Phi_h,\, \Phi - \Phi_h) = a(z,\, \Phi - \Phi_h).$$

From the Galerkin orthogonality, Schwarz's inequality, Theorem 5.2, and the regularity, for $\forall\, z_h \in U_h$, we have

$$\begin{aligned} a(z,\, \Phi - \Phi_h) &= a(z - z_h,\, \Phi - \Phi_h) \\ &\leq |z - z_h|_{H^1(\Omega)} |\Phi - \Phi_h|_{H^1(\Omega)} \\ &\leq C\, h\, |z|_{H^2(\Omega)} |\Phi - \Phi_h|_{H^1(\Omega)} \\ &\leq C\, h\, \|\Phi - \Phi_h\|_{L^2(\Omega)} |\Phi - \Phi_h|_{H^1(\Omega)}. \end{aligned}$$

Using Theorem 5.2 again and an analysis similar to Theorem 5.2, we get

$$\begin{aligned} \|\Phi - \Phi_h\|_{L^2(\Omega)} &\leq C\, h\, |\Phi - \Phi_h|_{H^1(\Omega)} \\ &\leq C\, h^{k+1}\, |\Phi|_{H^{k+1}(\Omega)}. \end{aligned}$$

□

5.4. Error estimates in the L^∞ norm

We will discuss the L^∞ the norm error estimation for the case when $k = 1$ and $k \geq 2$.

First, we estimate the L^∞ norm of Wang-Ball elements of order $k = 1$. Let the Green function w be defined by the following duality:

$$-\nabla^2 w = \delta, \quad \text{in } \Omega, \tag{5.9}$$

where δ is a Dirac distribution with singularity at $x_0 \in \Omega$.

Similarly, we can also obtain the variational formulation and Galerkin formulation, respectively,

$$\begin{aligned} a(w, v) &= v(x_0) \quad \forall v \in H_0^1, \\ a(w_h, v) &= v(x_0) \quad \forall v \in U_{h_0}. \end{aligned} \tag{5.10}$$

Before estimating the L^∞ norm, we provide a lemma.

Lemma 5.3. *[33] Let w and w_h be the solutions of Eqs (5.9) and (5.10), respectively, for $x_0 \in \Omega$ and $k = 1$. In this case, a constant $C > 0$ independent of x_0 exists such that*

$$\|w - w_h\|_{W_1^1(\Omega)} \leq C\, h\, |log\, h|.$$

Theorem 5.4. *Let Φ_h be the solution of the Galerkin formulation (4.6). Assume that the exact solution of Eq (4.1) satisfies $\Phi \in H^2(\Omega)$. Then for $k = 1$, a constant $C > 0$ independent of h exists, such that*

$$\|\Phi - \Phi_h\|_{L^\infty(\Omega)} \leq C\, h^{k+1}\, |log\, h|\, |\Phi|_{W_\infty^{k+1}(\Omega)}.$$

Proof. Since $a(v, \Phi - \Phi_h) = 0$, $\forall v \in U_{h_0}$, and the bilinear form $a(\cdot, \cdot)$ is bounded (that is, $\exists \beta > \infty$), such that

$$|a(v, w)| \leq \beta\, \|v\|_H \|w\|_H \quad \forall v,\, w \in H,$$

by Eq (5.10), we have

$$\begin{aligned} (\Phi - \Phi_h)(x_0) &= a(w, \Phi - \Phi_h) \\ &= a(w - w_h, \Phi - \Phi_h) \\ &= a(w - w_h, \Phi - v) \\ &\leq \beta\, \|w - w_h\|_{W_1^1(\Omega)} \|\Phi - v\|_{W_\infty^1(\Omega)}. \end{aligned}$$

Then by $\|\Phi - v\|_{W_\infty^1(\Omega)} \leq C\, h^k\, |\Phi|_{W_\infty^{k+1}(\Omega)}$ [33] and Lemma 5.3, we get

$$\sup_\Omega |\Phi - \Phi_h| \leq C\, h^{k+1}\, |log\, h|\, |\Phi|_{W_\infty^{k+1}(\Omega)}.$$

This theorem has been proven. □

Next, we consider the situation of $k \geq 2$. First, we consider the projection operator P_h

$$P_h : \Phi \in H^1(\Omega) \to P_h\Phi \in U_h,$$

associated with the inner product $a(\cdot, \cdot)$ of Eq (4.2). We also have

$$a(P_h\Phi, v) = a(\Phi, v) \quad \forall v \in U_{h_0}.$$

In addition, for the solution Φ_h of the Galerkin formulation (4.6) and the exact solution Φ of Eq (4.1), we have $\Phi_h = P_h\Phi$.

Theorem 5.5. *Let Φ_h be the solution of the Galerkin formulation (4.6). Assume that the exact solution of Eq (4.1) satisfies $\Phi \in H^2(\Omega)$. Then for $k \geq 2$, a constant C independent of h exists such that*

$$\|\Phi - \Phi_h\|_{L^\infty(\Omega)} \leq C\, h^{k+1}\, |\Phi|_{W_\infty^{k+1}(\Omega)}. \tag{5.11}$$

Proof. Since P_h is the projection operator, we have

$$\Phi - \Phi_h = \Phi - P_h\Phi = (I - P_h)(\Phi - v_h) \quad \forall v_h \in U_{h_0}.$$

By combining the inequality $\|P_h\Phi\|_{L^\infty(\Omega)} \leq C\,\|\Phi\|_{L^\infty(\Omega)}$ [34] and for $k \geq 2$, $\|\Phi - P_h\Phi\|_{L^\infty(\Omega)} \leq C\, h^{k+1}\,\|\Phi\|_{W_\infty^{k+1}(\Omega)}$ [34], we obtain

$$\begin{aligned}\|\Phi - \Phi_h\|_{L^\infty(\Omega)} &\leq \|\Phi - v_h\|_{L^\infty(\Omega)} + \|P_h(\Phi - \Phi_h)\|_{L^\infty(\Omega)} \\ &\leq C\,\|\Phi - v_h\|_{L^\infty(\Omega)} \\ &\leq C\, h^{k+1}\, |\Phi|_{W_\infty^{k+1}(\Omega)}.\end{aligned}$$

□

In this section, we give the definition of the Wang-Ball operator and derive the error estimation in the H^1-semi, L^2, and L^∞ norms. In the next section, we present several numerical examples to see that they are consistent with the error estimation.

6. Numerical examples

In this section, we solve several numerical examples under different electrostatics backgrounds and we verify that the numerical results are consistent with the error estimation in the previous section.

Example 6.1. *In the electrostatic field simulation, the problem of the electric field distribution inside a flat plate capacitor is assumed. Suppose the rectangular domain $\Omega = [0, 1] \times [0, 1]$ is inside the flat plate capacitor with $\Gamma_N = \varnothing$,*

$$\begin{cases} -\nabla^2\Phi = f, \\ \Phi\,|_{\partial\Omega} = 0, \end{cases}$$

where the electric potential is

$$\Phi(x, y) = x(2 - 5x^3 + 3x^2)(y^2 - y).$$

Through calculation, it is known that the charge density is as follows:

$$\rho(x, y) = -\epsilon_0(2(y - y^2)(6x - 15x^2) - 2x(2 - 5x^3 + 3x^2) - x(y - y^2)(30x - 6)).$$

It shows that within a certain region, when the electric potential distribution is Φ, the charge density is distributed according to ρ.

Table 1 shows a comparison of numerical errors under different degrees of the Wang-Ball basis functions and a mesh size h obtained by the FEM with the Wang-Ball element of Φ in the H^1-semi, L^2, and L^∞ norms. Moreover, we also calculate the convergence order of these errors.

Table 1. Comparison of the numerical errors of Φ in the H^1-semi, L^2, and L^∞ norms of the Dirichlet boundary in 2D.

Basis	h_1	h_2	$\lvert\Phi-\Phi_h\rvert_{H^1}$	Order	$\lVert\Phi-\Phi_h\rVert_{L^2}$	Order	$\lVert\Phi-\Phi_h\rVert_{L^\infty}$	Order
2×2 Wang-Ball	$\frac{1}{2}$	$\frac{1}{2}$	$9.0724e-02$	–	$6.6370e-03$	–	$1.8781e-02$	–
	$\frac{1}{4}$	$\frac{1}{4}$	$2.3051e-02$	1.9767	$8.7720e-04$	2.9196	$2.7679e-03$	2.7624
	$\frac{1}{8}$	$\frac{1}{8}$	$5.7820e-03$	1.9952	$1.1114e-04$	2.9805	$3.7231e-04$	2.8942
	$\frac{1}{16}$	$\frac{1}{16}$	$1.4466e-03$	1.9989	$1.3939e-05$	2.9952	$4.8213e-05$	2.9496
3×3 Wang-Ball	$\frac{1}{2}$	$\frac{1}{2}$	$8.7420e-03$	–	$4.4484e-04$	–	$9.3447e-04$	–
	$\frac{1}{4}$	$\frac{1}{4}$	$1.0819e-03$	3.0144	$2.8234e-05$	3.9778	$6.0437e-05$	3.9506
	$\frac{1}{8}$	$\frac{1}{8}$	$1.3490e-04$	3.0036	$1.7729e-06$	3.9933	$3.8055e-06$	3.9893
	$\frac{1}{16}$	$\frac{1}{16}$	$1.6851e-05$	3.0010	$1.1095e-07$	3.9981	$2.3824e-07$	3.9976
4×4 Wang-Ball	$\frac{1}{2}$	$\frac{1}{2}$	$4.8551e-14$	–	$2.3925e-15$	–	$1.8728e-14$	–
	$\frac{1}{4}$	$\frac{1}{4}$	$3.8719e-14$	–	$1.2020e-15$	–	$9.1016e-15$	–
	$\frac{1}{8}$	$\frac{1}{8}$	$3.6472e-14$	–	$7.2171e-16$	–	$4.3307e-15$	–

It can be seen from Table 1 that when solving the Poisson equation using tensor product Wang-Ball basis functions, the errors in the H^1-semi, L^2, and L^∞ norms decrease as the mesh size h gets smaller. Moreover, as the degree of the Wang-Ball basis functions increases, the errors also decrease. When we use 3×3-degree Wang-Ball basis functions in this example, the data in the table show that the convergence order of the H^1-semi norm is $k=3$, while those of the L^2 and L^∞ norms are both $k+1=4$, which is consistent with the theoretical analysis in the previous section. A similar pattern holds for the 2×2-degree Wang-Ball basis functions. In addition, because the mesh refinement in this example decreases from $1/2$ to $1/16$ in multiples of $1/2$, for the H^1-semi norm and $k\times k$-degree Wang-Ball basis functions, the convergence order is $O(h^k)$. Therefore, as the mesh size decreases, the error values decrease by a factor of $(1/2)^k$.

Due to the precision of the computer, we can only calculate 4×4-degree Wang-Ball basis functions, and the errors in the L^2 norm can reach 10^{-16}, and those in the L^∞ norm can also reach 10^{-15}.

Example 6.2. *In the electromagnetic shielding design of a 2D plane, it is assumed that a rectangular shielding domain $\Omega=[0,1]\times[0,1]$ exists. Consider the Poisson equation with the Dirichlet boundary condition for the parts where the electric potential is known and fixed, and the Neumann boundary condition for the parts where the electric flux is known, as follows:*

$$\begin{cases} -\nabla^2\Phi = f, \\ \nabla\Phi\cdot\boldsymbol{n}\,|_{y=0} = p, \\ \Phi\,|_{\partial\Omega/\Gamma_N} = 0, \end{cases}$$

where the electric potential distribution function Φ within the shielding area is

$$\Phi(x, y) = -cos(2\pi x)sin(2\pi y) + sin(2\pi x),$$

and $\boldsymbol{n}$ *is the outward normal unit vector.*

The charge density ρ describes the spatial distribution of charges within the shielding region, namely

$$\rho(x, y) = \epsilon_0(8\pi^2 cos(2\pi x)sin(2\pi y) - 4\pi^2 sin(2\pi y)).$$

The comparison of the numerical errors of solving the Poisson equation with different degrees of Wang-Ball basis functions in the H^1-semi, L^2, and L^∞ norms are shown in Table 2. Furthermore, we also calculate the convergence order of the data in this table and we have generated the corresponding graphical illustrations shown in Figure 6.

The FEM using the Wang-Ball basis functions is effective in improving the solutions' accuracy. After inspecting the numerical data in Table 2, as the degree of the Wang-Ball basis functions increases, the errors become smaller under the same mesh size h. Furthermore, we can know from Figure 6 that as the mesh size h reduces, so do the values of the numerical errors. As the degree of the Wang-Ball basis functions increases, the trend of decreasing error values becomes more evident.

As can be seen from Table 2, it can be observed that the numerical results indicate that the convergence order of Φ is $O(h^k)$ in the H^1-semi norm for the high-order Wang-Ball elements and $O(h^{k+1})$ in both the L^2 and L^∞ norms. Therefore, we can deduce that the convergence order is consistent with the error estimation, indicating the reliability and consistency of this method.

Table 2. Comparison of the numerical errors of Φ in the H^1-semi, L^2, and L^∞ norms of the mixed boundary in 2D.

Basis	h_1	h_2	$\lvert\Phi - \Phi_h\rvert_{H^1}$	Order	$\lVert\Phi - \Phi_h\rVert_{L^2}$	Order	$\lVert\Phi - \Phi_h\rVert_{L^\infty}$	Order
2×2 Wang-Ball	$\frac{1}{4}$	$\frac{1}{4}$	$5.6510e-01$	–	$2.0923e-02$	–	$4.8958e-02$	–
	$\frac{1}{8}$	$\frac{1}{8}$	$1.4369e-01$	1.9755	$2.7434e-03$	2.9311	$7.3925e-03$	2.7274
	$\frac{1}{16}$	$\frac{1}{16}$	$3.6064e-02$	1.9943	$3.4693e-04$	2.9832	$9.6095e-04$	2.9435
4×4 Wang-Ball	$\frac{1}{4}$	$\frac{1}{4}$	$7.4321e-03$	–	$1.4848e-04$	–	$4.1581e-04$	–
	$\frac{1}{8}$	$\frac{1}{8}$	$4.7188e-04$	3.9773	$4.7429e-06$	4.9684	$1.3958e-05$	4.8968
	$\frac{1}{16}$	$\frac{1}{16}$	$2.9609e-05$	3.9943	$1.4904e-07$	4.9920	$4.3972e-07$	4.9884
6×6 Wang-Ball	$\frac{1}{4}$	$\frac{1}{4}$	$3.8680e-05$	–	$5.3072e-07$	–	$1.4694e-06$	–
	$\frac{1}{8}$	$\frac{1}{8}$	$6.1219e-07$	5.9815	$4.2109e-09$	6.9777	$1.2510e-08$	6.8760
	$\frac{1}{16}$	$\frac{1}{16}$	$9.6111e-09$	5.9931	$3.3859e-11$	6.9584	$1.0441e-10$	6.9047

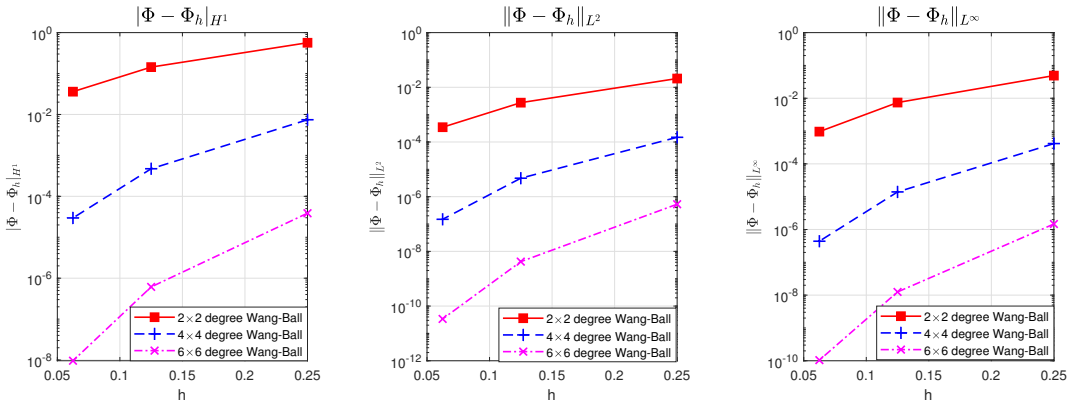

Figure 6. Comparison of the numerical errors of Φ in 2D.

Example 6.3. *In the analysis of a 3D geological structure* $\Omega = [0, 1] \times [0, 1] \times [0, 1]$*, it is assumed that there is an electric potential difference between different mineral layers.*

$$\begin{cases} -\nabla^2\Phi = f, \\ \Phi\,|_{\partial\Omega} = 0, \end{cases}$$

where $\Gamma_N = \varnothing$*. The electric potential distribution function* Φ *within this geological structure is*

$$\Phi(x, y, z) = xyzsin(\pi x)sin(\pi y)sin(\pi z),$$

and the equivalent charge distribution ρ *in the underground area is*

$$\begin{aligned}\rho(x, y, z) =& \varepsilon_0(2xy\pi cos(\pi z)sin(\pi x)sin(\pi y) + 2xz\pi cos(\pi y)sin(\pi x)sin(\pi z) \\ &+ 2yz\pi cos(\pi x)sin(\pi y)sin(\pi z) - 3xyz\pi^2 sin(\pi x)sin(\pi y)sin(\pi z)).\end{aligned}$$

The numerical errors and the convergence order acquired by the FEM utilizing the Wang-Ball basis functions in the H^1*-semi,* L^2*, and* L^∞ *norms are presented in Table 3. At the same time, we have created the corresponding graphs, which are shown in Figure 7.*

Table 3. Comparison of the numerical errors of Φ in the H^1-semi, L^2, and L^∞ norms of the Dirichlet boundary in 3D.

Basis	h_1	h_2	h_3	$\lvert\Phi-\Phi_h\rvert_{H^1}$	Order	$\lVert\Phi-\Phi_h\rVert_{L^2}$	Order	$\lVert\Phi-\Phi_h\rVert_{L^\infty}$	Order
1×1×1 Wang-Ball	$\frac{1}{4}$	$\frac{1}{4}$	$\frac{1}{4}$	$1.1968e-01$	–	$7.3591e-03$	–	$3.5838e-02$	–
	$\frac{1}{8}$	$\frac{1}{8}$	$\frac{1}{8}$	$5.8549e-02$	1.0315	$1.7776e-03$	2.0496	$1.0193e-02$	1.8139
	$\frac{1}{16}$	$\frac{1}{16}$	$\frac{1}{16}$	$2.9134e-02$	1.0069	$4.4041e-04$	2.0130	$2.5252e-03$	2.0131
2×2×2 Wang-Ball	$\frac{1}{4}$	$\frac{1}{4}$	$\frac{1}{4}$	$1.2252e-02$	–	$4.5374e-04$	–	$1.9894e-03$	–
	$\frac{1}{8}$	$\frac{1}{8}$	$\frac{1}{8}$	$3.1023e-03$	1.9816	$5.9225e-05$	2.9376	$2.8441e-04$	2.8063
	$\frac{1}{16}$	$\frac{1}{16}$	$\frac{1}{16}$	$7.7756e-04$	1.9963	$7.4796e-06$	2.9852	$3.6220e-05$	2.9731
3×3×3 Wang-Ball	$\frac{1}{4}$	$\frac{1}{4}$	$\frac{1}{4}$	$1.2691e-03$	–	$2.5996e-05$	–	$1.6188e-04$	–
	$\frac{1}{8}$	$\frac{1}{8}$	$\frac{1}{8}$	$1.5786e-04$	3.0071	$1.6533e-06$	3.9749	$1.0921e-05$	3.8897
	$\frac{1}{16}$	$\frac{1}{16}$	$\frac{1}{16}$	$1.9710e-05$	3.0016	$1.0388e-07$	3.9924	$7.1472e-07$	3.9336

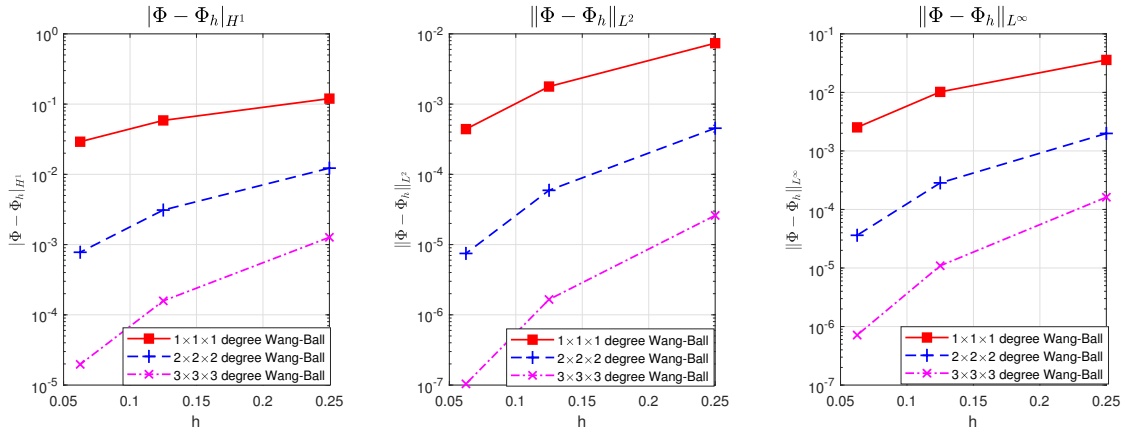

Figure 7. Comparison of the numerical errors of Φ in 3D.

In this example, we use the Wang-Ball basis functions of degree $k \times k \times k$ to solve the Poisson equation. It can be seen from Table 3 that as k increases from 1 to 3, the errors become smaller. Moreover, as the mesh size h decreases, from 1/4 to 1/16, the errors also gradually decrease. We can say that both the increase in the degrees of the Wang-Ball basis functions and the gradual refinement of the mesh can improve the computational accuracy. The convergence order of the solutions Φ within the H^1-semi norm is characterized by k-order convergence $O(h^k)$. In the context of the L^2 and L^∞ norms of high-order Wang-Ball elements, the convergence order of Φ is $k+1$-order convergence $O(h^{k+1})$.

In addition, as shown in the three graphs presented in Figure 7, as the mesh size h decreases, the three lines in each graph decrease at different rates. Among them, the line representing the $3 \times 3 \times 3$-degree Wang-Ball basis functions has the largest rate of decline, which means that the speed at which the errors decrease is accelerating compared with the other degrees.

The main purpose of this section is to evaluate the feasibility and effectiveness of the FEM with Wang-Ball elements, thereby validating its suitability for numerical computations. These examples have illustrated that the convergence order is consistent with the error estimation.

7. Conclusions and future work

In order to solve the classical equation in electrostatics, the Poisson equation, we use a new type of basis functions in the FEM, the Wang-Ball basis functions. In this paper, we provide the definition of Wang-Ball elements and employ the FEM with these elements to solve the Poisson equation with mixed boundary conditions. Our method involves constructing the trial and test function spaces to derive the Galerkin formulation. We then provide the definition of the Wang-Ball operator and combine the averaged version of Taylor polynomials to derive error estimates in the H^1-semi, L^2, and L^∞ norms.

Furthermore, we have provided a series of numerical examples under different electrostatics backgrounds, and we have solved the Poisson equation using high-degree Wang-Ball basis functions. It has been illustrated by these examples that the convergence order is in line with the error estimates.

When there is no free charge distribution in the region under study, that is, the charge density $\rho = 0$, the Poisson equation simplifies to the Laplace equation $\nabla^2\Phi = 0$. This equation describes the distribution law of the electrostatic potential in the charge-free region. In many practical problems (for example, when solving electrostatic field problems with a certain degree of symmetry), the Laplace equation plays an important role. In subsequent research, we will use the Wang-Ball basis functions to solve the Laplace equation.

Meanwhile, since the Poisson equation in electrostatics is a steady-state special case of time-dependent electromagnetic problems, the study of time-dependent equations requires further integration of space-time discretization theories. Related work will focus on coupled modeling of the dynamic charge distribution and electromagnetic field propagation. In subsequent studies, we will employ Wang-Ball basis functions to investigate time-dependent evolution equations. In addition, the numerical examples presented in this paper are all conducted in regular domains. The solution of irregular domains is typically carried out on Cartesian grids. In the next step of the research, we will also consider solving equations over irregular domains by using Cartesian grids.

Author contributions

Lanyin Sun: Writing-review and editing, methodology, funding acquisition, conceptualization, visualization; Ziwei Dong: Writing-original draft, software, data curation. All authors have read and approved the final version of the manuscript for publication.

Use of Generative AI tools declaration

The authors declare they have not used artificial intelligence (AI) tools in the creation of this article.

Acknowledgments

The authors are very grateful to the editor and anonymous referees for their valuable comments and constructive suggestions, which helped to improve the paper significantly. This work is partly supported by Natural Science Foundation of Henan (No. 252300420348).

Conflict of interest

The authors declare that there are no conflicts of interest.

References

1. P. Koehl, Electrostatics calculations: Latest methodological advances, *Curr. Opin. Struct. Biol.*, **16** (2006), 142–151. https://doi.org/10.1016/j.sbi.2006.03.001
2. B. D. Storey, M. Z. Bazant, Effects of electrostatic correlations on electrokinetic phenomena, *Phys. Rev. E*, **86** (2012), 056303. https://doi.org/10.1103/PhysRevE.86.056303
3. C. Berti, D. Gillespie, J. P. Bardhan, R. S. Eisenberg, C. Fiegna, Comparison of three-dimensional Poisson solution methods for particle-based simulation and inhomogeneous dielectrics, *Phys. Rev. E*, **86** (2012), 011912. https://dx.doi.org/10.1103/PhysRevE.86.011912
4. S. Srebrenik, H. Weinstein, R. Pauncz, Analytical calculation of atomic and molecular electrostatic potentials from the Poisson equation, *Chem. Phys. Lett.*, **20** (1973), 419–423. https://doi.org/10.1016/0009-2614(73)85188-7
5. J. E. Schnitzer, K. C. Lambrakis, Electrostatic potential and born energy of charged molecules interacting with phosholipid membranes: Calculation via 3-D numerical solution of the full poisson equation, *J. Theor. Biol.*, **152** (1991), 203–222. https://doi.org/10.1016/S0022-5193(05)80453-9
6. V. P. H. Hu, Y. S. Wu, P. Su, Investigation of electrostatic integrity for ultra-thin-body GeOI MOSFET using analytical solution of Poisson's equation, In: *2008 IEEE international conference on electron devices and solid-state circuits*, 2008, 1–4. http://dx.doi.org/10.1109/EDSSC.2008.4760684
7. M. Salem, O. Aldabbagh, Numerical solution to Poisson's equation for estimating electrostatic properties resulting from an axially symmetric gaussian charge density distribution: Charge in free space, *Mathematics*, **12** (2024), 1948. http://dx.doi.org/10.3390/math12131948
8. I. H. Tan, G. L. Snider, L. D. Chang, E. L. Hu, A self-consistent solution of Schrödinger-Poisson equations using a nonuniform mesh, *J. Appl. Phys.*, **68** (1990), 4071–4076. https://doi.org/10.1063/1.346245
9. F. Dou, Y. Liu, C. S. Chen, The method of particular solutions for solving nonlinear Poisson problems, *Comput. Math. Appl.*, **77** (2019), 501–513. https://doi.org/10.1016/j.camwa.2018.09.053
10. D. N. Arnold, An interior penalty finite element method with discontinuous elements, *SIAM J. Numer. Anal.*, **19** (1982), 742–760. https://doi.org/10.1137/0719052

11. J. M. Guedes, N. Kikuchi, Preprocessing and postprocessing for materials based on the homogenization method with adaptive finite element methods, *Comput. Methods Appl. Mech. Eng.*, **83** (1990), 143–198. https://doi.org/10.1016/0045-7825(90)90148-F
12. T. Strouboulis, I. Babuška, K. Copps, The design and analysis of the generalized finite element method, *Comput. Methods Appl. Mech. Eng.*, **181** (2000), 43–69. https://doi.org/10.1016/S0045-7825(99)00072-9
13. A. Logg, Automating the finite element method, *Arch. Comput. Methods Eng.*, **14** (2007), 93–138. https://doi.org/10.1007/s11831-007-9003-9
14. A. Baghbani, H. Baghbani, M. M. Shalchiyan, K.Kiany, Utilizing artificial intelligence and finite element method to simulate the effects of new tunnels on existing tunnel deformation, *J. Comput. Cogn. Eng.*, **3** (2024), 166–175. https://doi.org/10.47852/bonviewJCCE2202307
15. C. M. Cortis, R. A. Friesner, Numerical solution of the Poisson-Boltzmann equation using tetrahedral finite-element meshes, *J. Comput. Chem.*, **18** (1997), 1591–1608. https://doi.org/10.1002/(SICI)1096-987X(199710)18:13¡1591::AID-JCC3¿3.0.CO;2-M
16. K. H. Hsu, P. Y. Chen, C. T. Hung, L. H. Chen, J. S. Wu, Development of a parallel Poisson's equation solver with adaptive mesh refinement and its application in field emission prediction, *Comput. Phys. Commun.*, **174** (2006), 948–960. https://doi.org/10.1016/j.cpc.2006.01.006
17. M. Holst, J. A. Mccammon, Z. Yu, Y. C. Zhou, Y. Zhu, Adaptive finite element modeling techniques for the Poisson-Boltzmann equation, *Commun. Comput. Phys.*, **11** (2012), 179–214. https://doi.org/10.4208/cicp.081009.130611a
18. H. Gao, P. Sun, A linearized local conservative mixed finite element method for Poisson-Nernst-Planck equations, *J. Sci. Comput.*, **77** (2018), 793–817. https://doi.org/10.1007/s10915-018-0727-5
19. Z. Guo, F. Lan, H. Lai, X. Yang, F. Xiao, Z. Wang, et al., A finite element analysis for vacuum amplifier electron gun of fine pencil beam, *IEEE Trans. Electron Devices*, **71** (2024), 3201–3208. http://dx.doi.org/10.1109/TED.2024.3377196
20. C. de Boor, On calculating with B-splines, *J. Approx. Theory*, **6** (1972), 50–62. https://doi.org/10.1016/0021-9045(72)90080-9
21. M. G. Cox, The numerical evaluation of B-splines, *IMA J. Appl. Math.*, **10** (1972), 134–149. https://doi.org/10.1093/imamat/10.2.134
22. P. Kagan, A. Fischer, P. Z. Bar-Yoseph, New B-spline finite element approach for geometrical design and mechanical analysis, *Int. J. Numer. Methods Eng.*, **41** (1998), 435–458. https://doi.org/10.1002/(SICI)1097-0207(19980215)41:3¡435::AID-NME292¿3.0.CO;2-U
23. T. J. R. Hughes, J. A. Cottrell, Y. Bazilevs, Isogeometric analysis: CAD, finite elements, NURBS, exact geometry and mesh refinement, *Comput. Methods Appl. Mech. Eng.*, **194** (2005), 4135–4195. https://doi.org/10.1016/j.cma.2004.10.008
24. T. N. T. Goodman, H. B. Said, Shape preserving properties of the generalised Ball basis, *Comput. Aided Geom. D.*, **8** (1991), 115–121. https://doi.org/10.1016/0167-8396(91)90037-C
25. H. B. Said, A generalized Ball curve and its recursive algorithm, *ACM Trans. Graph.*, **8** (1989), 360–371. https://doi.org/10.1145/77269.77275

26. T. N. T. Goodman, H. B. Said, Properties of generalized Ball curves and surfaces, *Comput. Aided Des.*, **23** (1991), 554–560. https://doi.org/10.1016/0010-4485(91)90056-3

27. S. M. Hu, G. Z. Wang, T. G. Jin, Properties of two types of generalized Ball curves, *Comput. Aided Des.*, **28** (1996), 125–133. https://doi.org/10.1016/0010-4485(95)00047-X

28. L. Zhang, J. Tan, H. Wu, Z. Liu, The weighted dual functions for Wang-Bézier type generalized Ball bases and their applications, *Appl. Math. Comput.*, **215** (2009), 22–36. https://doi.org/10.1016/j.amc.2009.04.026

29. Y. F. Hamza, M. F. Hamza, A. Rababah, S. Ibrahim, Geometric degree reduction of Wang-Ball curves, *Appl. Comput. Intell. Soft Comput.*, **2023** (2023), 5483111. https://doi.org/10.1155/2023/5483111

30. S. C. Brenner, L. R. Scott, *The mathematical theory of finite element methods*, 3 Eds., New York: Springer, 2008. https://doi.org/10.1007/978-0-387-75934-0

31. P. G. Ciarlet, *The finite element method for elliptic problems*, Philadelphia: SIAM Publications, 2002. https://doi.org/10.1137/1.9780898719208

32. G. Wu, F. Wang, L. Qiu, Physics-informed neural network for solving Hausdorff derivative Poisson equations, *Fractals*, **31** (2023), 2340103. https://doi.org/10.1142/S0218348X23401035

33. R. Scott, Optimal L^∞ estimates for the finite element method on irregular meshes, *Math. Comput.*, **30** (1976), 681–697. https://doi.org/10.2307/2005390

34. J. A. Nitsche, L_∞-convergence of finite element approximation, *Publ. Sém. Math. Inf.*, **S3** (1975), 1–17.

AIMS Press